

Mass Reversal Effect in the Split Indirect Exciton of Ge

A. Frova,* G. A. Thomas, R. E. Miller, and E. O. Kane

Bell Laboratories, Murray Hill, New Jersey 07974

(Received 29 January 1975)

Experimental and theoretical evidence is reported of hybridization effects leading to strong nonparabolicity in the E - K dispersion curves of the Ge anisotropy-split excitons. The measured density of states indicates substantial deviation from ideal-gas behavior even at a few kelvins. A splitting of 1.01 ± 0.03 meV is measured.

In an earlier paper by one of the authors¹ it has been noted that the transverse translational masses of the upper and lower 1s indirect excitons in germanium "reverse" as the transverse kinetic energy increases. This "mass reversal" effect leads to substantial nonparabolicity in the density of states which we have confirmed experimentally. By means of high-resolution wavelength-derivative transmission measurements, a precise determination is also obtained of the exciton splitting, of the oscillator strengths, and of an upper limit for the intrinsic line broadening. These parameters were previously determined with large uncertainty²⁻⁴ and in some cases they were an indirect result of the analysis of the line shape of free-exciton luminescence,^{5,6} or of the thermal-activation energy of microwave absorption.⁷ As the mass-reversal effect to be described here

causes the excitonic absorption line shape to deviate from the ideal square-root dependence on energy, the present results bear an immediate consequence on other problems, such as the determination of the work function for the evaporation of free excitons from the electron-hole-drop state.^{8,9} In addition, they allow an estimate of the limits of accuracy for Ge of the theoretical approaches to the determination of the exciton splitting and of the E - K dispersion relations.

The experiment was performed on a 7-mm-long sample, chemically etched following mechanical polishing. The sample was held suspended in an exchange-gas cryostat, cooled to 1.1°K, and illuminated by monochromatic light. Wavelength modulation was achieved by off-axis rotation of a 1.5-mm-thick quartz disk, placed in the monochromator at the exit slit, and producing a light-

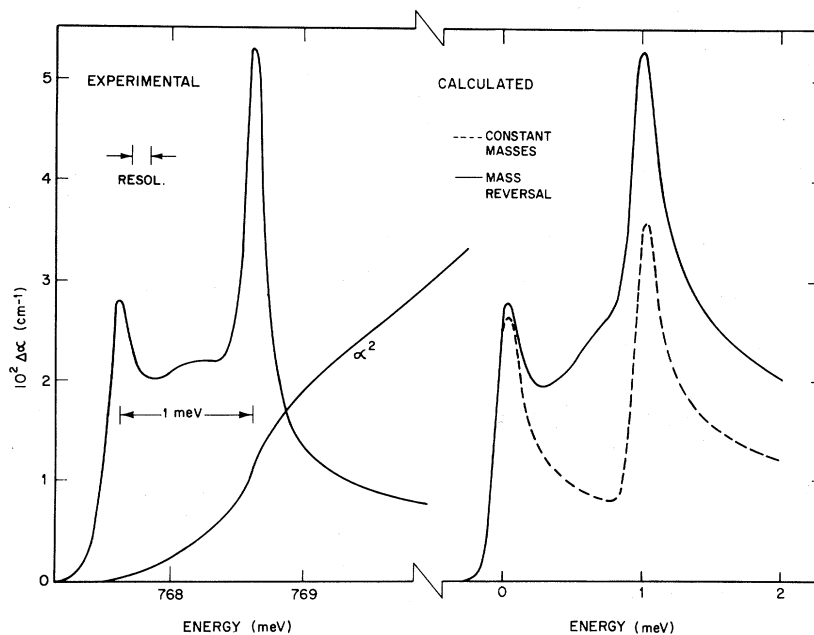


FIG. 1. Experimental and calculated wavelength-modulation spectra of the absorption coefficient for LA-phonon-assisted transitions at 1.1°K. Also shown is the square of the measured absorption coefficient, which clearly illustrates the nonparabolicity resulting from the mass-reversal effect.

TABLE I. Experimental and variational exciton binding energies in Ge (meV).

| | Experiment | McLean and Loudon | | Zwerdling <i>et al.</i> | |
|----------------------------|-------------------|-------------------|-------|-------------------------|-------|
| | | (old) | (new) | (old) | (new) |
| $ E_-(0) $ | 4.15 ^a | 3.47 | 4.17 | 2.91 | 3.50 |
| $ E_+(0) $ | 3.14 | 2.88 | 3.25 | 2.36 | 2.66 |
| $\Delta = E_+(0) - E_-(0)$ | 1.01 ± 0.03 | 0.59 | 0.92 | 0.55 | 0.84 |

^aFrom Ref. 10.

beam displacement approximately equal to the slit width. The transmitted intensity I and its modulation ΔI were simultaneously recorded. A spectrum of the modulated absorption coefficient $\Delta\alpha \sim \Delta I/I$, for the LA-phonon-assisted transitions, is shown on the left-hand side of Fig. 1, along with the square of its absolute contribution to the value of α . Both curves are immediately suggestive of a deviation from the square-root functional dependence of α on energy, characteristic of parabolic bands. The discrepancy is particularly evident in the region between the two singularities. The widths of the peaks are essentially determined by the spectrometer resolution of 0.16 meV; they establish an upper limit for the the intrinsic broadening of the exciton, which is rather smaller than that inferred from the analysis of the free-exciton luminescence line shape in terms of parabolic bands.¹⁰ It should be emphasized that the strongly asymmetric shape of the spectrum on the two sides of each peak causes the apparent splitting to become rapidly smaller when the resolution is made poorer (we have measured about 0.9 meV by just doubling the slit widths).

The experimental results are summarized in Table I. Our splitting value is consistent with earlier absorption spectra; however, our data are far less affected by spurious effects, such as poor resolution² and strain.³ The binding energy $E_-(0)$ for the lower exciton is the most reliable experimental datum available and comes from photoconductivity measurements extrapolated to zero electric field.¹¹ Combining this with the present value for Δ , we deduce for the shallower exciton $E_+(0) = 3.14$ meV.

For a more complete understanding of the data we shall now briefly describe the theoretical picture. Perturbation methods^{1,12} are inaccurate for germanium and variational results^{13,14} are rather incomplete. In order to construct a reasonable

approximate description, we choose an analytic form for the dispersion relations suggested by the perturbation results. This form may be more generally justified as representing the coupling of two exciton states through terms quadratic in the total momentum \vec{K} :

$$E_{\pm}(\vec{K}) = E_s + (\hbar^2/2m_0)(K_i^2 r_{is} + K_t^2 r_{ts}) \pm Z, \quad (1)$$

$$Z = [A^2 + (\hbar^2/2m_0)^2(r_{tc}^2 K_t^4 + r_{mc}^2 K_t^2 K_i^2)]^{1/2}, \quad (2)$$

$$A = E_d + (\hbar^2/2m_0)(K_i^2 r_{id} + K_t^2 r_{td}). \quad (3)$$

K_i and K_t are the exciton momenta parallel and perpendicular to the ellipsoidal axis of the conduction band. The exciton splitting is $\Delta = 2E_d$ and the r 's are reciprocal masses, in units of m_0^{-1} , as determined later from Eqs. (4) and (5) and Ref. 14. The states + (−) can be classified group theoretically as L_6^+ ($L_4^+ + L_5^+$)¹² or $\pm \frac{1}{2}$ ($\pm \frac{3}{2}$) in terms of angular momentum components. Theoretical estimates of $E_{\pm}(0)$ have been obtained variationally by McLean and Loudon.¹³ A much simpler "single-band" variational scheme was proposed by Zwerdling *et al.*¹⁴ whose results are also shown in Table I for the best current parameters (Table II) and for the parameters used by McLean and Loudon. Table I also gives improved McLean and Loudon values for the better parameters, as obtained by linear scaling. This gives a splitting of 0.92 meV, to be compared to the experimental value of 1.01 meV. We employ the experimental value in Eq. (1), however. The method of Zwerdling *et al.* also leads directly to ex-

TABLE II. Cyclotron mass parameters.

| ϵ | γ_1 | γ_2 | γ_3 | m_l | m_t |
|------------|------------|------------|------------|-------|---------|
| 15.36 | 13.38 | 4.24 | 5.69 | 1.588 | 0.08152 |

TABLE III. Exciton masses.

| | Low K , Eq. (5) | High K , Eq. (6) | High K , Eq. (1) | Reduced masses |
|----------|----------------------|-----------------------|-----------------------|-------------------|
| M_{i-} | 2.09 | 2.09 | 2.09 | 0.380 |
| M_{i+} | 1.63 | 1.63 | 1.63 | 0.0394 |
| M_{t-} | 0.134 | 0.459 | 0.459 | 0.0319 |
| M_{t+} | 0.211 | 0.123 | 0.0998 | 0.0500 |

pressions for the translational masses,

$$\begin{aligned} M_{i\pm} &= (r_{is} + r_{id})^{-1} = m_i + (\gamma_1 \pm 2\gamma_3)^{-1}, \\ M_{t\pm} &= (r_{ts} \pm r_{td})^{-1} = m_t + (\gamma_1 \mp \gamma_3)^{-1}, \end{aligned} \quad (4)$$

by use of a center-of-mass transformation for the the different bands treated independently. Analogous expressions for the reduced masses lead to the binding energies of Zwerdling *et al.* Both translational and reduced masses are listed in Table III. The above expressions can be interpreted in terms of light- and heavy-hole masses for the [111] direction:

$$m_{1h}^{-1}(111) = \gamma_1 + 2\gamma_3, \quad m_{1h}^{-1}(\bar{1}\bar{1}\bar{1}) = \gamma_1 - 2\gamma_3.$$

In the direction of quantization (parallel), the E_- bands have heavy-hole masses while the E_+ bands have light-hole masses. In the perpendicular direction the situation is reversed. For degenerate bands it can be shown that the analog of the center-of-mass transformation is the minimization of the translational kinetic energy. For large \vec{K} this approach leads to light- and heavy-hole bands with the direction of quantization parallel to the average hole momentum. Equations (4) then become

$$\begin{aligned} M_{i-}' &= m_i + (\gamma_1 - 2\gamma_{\perp})^{-1} \\ &= [r_{ts} - (r_{td}^2 + r_{tc}^2)^{1/2}]^{-1}, \\ M_{i+}' &= m_i + (\gamma_1 + 2\gamma_{\perp})^{-1}, \\ M_{t\pm}' &= M_{i\pm}; \quad \gamma_{\perp} = (3\gamma_3^2/4 + \gamma_2^2/4)^{1/2}. \end{aligned} \quad (5)$$

In K_i directions, the masses remain unchanged and there is no nonparabolicity. Along K_t the $- (+)$ masses become heavy (light) because at high \vec{K} the direction of quantization follows the

average hole momentum instead of being fixed by the axis of the electron ellipsoid.¹⁵ At low \vec{K} the energy minimization is dominated by the exciton binding energy which in turn depends on the reduced masses listed in Table III. Clearly binding is favored by aligning the heavy-hole direction with the heavy-electron direction to produce a heavy reduced mass. At large \vec{K} the translational kinetic energy dominates the energy minimization and the quantization direction follows the direction of the average hole momentum. (The average hole momentum is only parallel to \vec{K} for $\vec{K} \parallel \vec{K}_t$ or $\vec{K} \parallel K_i$ unless $m_i = m_t$.) The parameters in Table IV lead via Eq. (1) to the masses in columns 1 and 3 of Table III. We have too few available parameters to fit M_{t+} at high K . The discrepancy of 23% will affect the calculated spectra only at high energies. The mass-reversal effect is shown quantitatively by the values of $M_{t\pm}$ in columns 1 and 2 of Table III. The exciton Bohr radius a_0^* calculated directly from the method presented here is 127 Å, in good agreement with 114 Å from the measured binding energy using the hydrogenic formula.

The optical absorption is proportional to the density of states, derivable from Eq. (1), times an optical matrix element

$$S_{\pm}(\vec{K}=0) = S_s \pm S_d = |\varphi_{\pm}(0)|^2 |M_{\pm}|^2, \quad (6)$$

where $\varphi_{\pm}(0)$ is the amplitude of the envelope function at the origin and M_{\pm} is the phonon matrix element. The optical absorption is then

$$\alpha \sim \int d^3K [S_s \pm (A/Z)S_d] \delta(\hbar\omega - E_{\pm}(\vec{K})). \quad (7)$$

The relative values of S_s and S_d are chosen to fit experiment. Equation (7) has been evaluated numerically with the parameters shown in Table IV. The results, broadened with a Gaussian matching the experimental resolution, are shown in Fig. 1 as the solid line on the right-hand side. The dashed line is the parabolic density of states obtained by setting $r_{tc} = r_{mc} = 0$ in Eq. (1) but leaving the other parameters the same. The importance of nonparabolicity is striking.

Comparison of the experimental spectra with theory clearly indicates the occurrence of mass

TABLE IV. Dispersion parameters.

| E_d | r_{1s} | r_{ts} | r_{id} | r_{td} | r_{tc} | r_{mc} | S_s | S_d |
|-------|----------|----------|----------|----------|----------|----------|-------|-------|
| 0.505 | 0.547 | 6.10 | 0.068 | -1.37 | 3.67 | 0.848 | 0.88 | -0.12 |

reversal corresponding to hybridization. One obvious discrepancy is the extra breadth of the upper theoretical peak; however, in view of the oversimplified nature of the theory, the agreement is quite satisfactory.

*On leave from Istituto di Fisica, Università di Roma, Rome, Italy.

¹E. O. Kane, Phys. Rev. B **11**, 3850 (1975).

²E. F. Gross, V. J. Safarov, A. N. Titkov, and I. S. Shlimak, Pis'ma Zh. Eksp. Teor. Fiz. **13**, 332 (1971) [JETP Lett. **13**, 235 (1971)]; T. Nishino, M. Takeda, and Y. Hamakawa, J. Phys. Soc. Jpn. **37**, 1016 (1974).

³K. J. Button, L. M. Roth, W. H. Kleiner, S. Zwerdling, and B. Lax, Phys. Rev. Lett. **2**, 161 (1959).

⁴C. C. Macfarlane, T. P. McLean, J. E. Quarrington, and V. Roberts, Phys. Rev. **108**, 1377 (1957).

⁵C. Benoit à la Guillaume and M. Voos, Solid State Commun. **12**, 1257 (1973).

⁶T. K. Lo, Solid State Commun. **15**, 1231 (1974).

⁷E. M. Gershenson, G. N. Gol'tsman, and N. G. Ptitsina, Pis'ma Zh. Eksp. Teor. Fiz. **18**, 160 (1973) [JETP Lett. **18**, 93 (1973)]; E. M. Gershenson, in *Proceedings of the Twelfth International Conference on the Physics of Semiconductors, Stuttgart, Germany, 1974*,

edited by M. H. Pilkuhn (Teubner, Stuttgart, Germany), p. 355. See also V. S. Vavilov, N. V. Guzeev, V. A. Zayats, V. L. Konenko, G. S. Mandel'shtam, and V. N. Murzin, Pis'ma Zh. Eksp. Teor. Fiz. **17**, 480 (1973) [JETP Lett. **17**, 345 (1973)].

⁸G. A. Thomas, T. G. Phillips, T. M. Rice, and J. C. Hensel, Phys. Rev. Lett. **31**, 386 (1973).

⁹Ya. E. Pokrovskii, Phys. Status Solidi (a) **11**, 385 (1972).

¹⁰See, e.g., Ref. 5. This particular aspect of the mass-reversal effect will be treated in a forthcoming paper.

¹¹V. I. Sidorov and Ya. E. Pokrovskii, Fiz. Tech. Poluprov. **6**, 2405 (1972) [Sov. Phys. Semicond. **6**, 2015 (1973)].

¹²A. Baldereschi and N. O. Lipari, Phys. Rev. B **3**, 439 (1971); N. O. Lipari and A. Baldereschi, Phys. Rev. B **3**, 2497 (1971).

¹³T. P. McLean and R. Loudon, J. Phys. Chem. Solids **13**, 1 (1960).

¹⁴S. Zwerdling, B. Lax, L. M. Roth, and K. J. Button, Phys. Rev. **114**, 80 (1959).

¹⁵The masses are actually a continuous function of direction since the hole mass varies with direction. We do not attempt this refinement but use a simple ellipsoidal form with the masses as given in Eq. (5). The parameter r_{mc} in Eq. (1) is fixed by the assumption of ellipsoidal energy surfaces at high K .

Critical Dynamics of Isotropic Antiferromagnets in $4 - \epsilon$ Dimensions

R. Freedman

*Xerox Research Palo Alto Research Center, Palo Alto, California 94304, and
The James Franck Institute,* The University of Chicago, Chicago, Illinois 60637*

and

Gene F. Mazenko†

*W. W. Hansen Laboratories of Physics, Stanford University, Stanford, California 94304, and
The James Franck Institute* and The Department of Physics, The University of Chicago, Chicago, Illinois 60637*

(Received 31 March 1975)

The critical dynamics of a model isotropic antiferromagnet is studied in $4 - \epsilon$ dimensions above and at T_N . The renormalization-group, characteristic-frequency exponent, and shape function are determined to order ϵ . In particular we find fluctuation-induced peaks in the shape function at and above the Néel temperature. We find results in agreement with dynamical scaling.

In this Letter we discuss a model for the critical dynamics of an isotropic Heisenberg antiferromagnet. In contrast to the ferromagnet studied earlier,^{1,2} where the conventional theory holds only for $d > 6$, the antiferromagnet has simple critical dynamics for $d > 4$. We therefore use renormalization-group (RNG) techniques to analyze our model and perform a self-consistent calculation

to $O(\epsilon)$ ($\epsilon = 4 - d$) for $T \geq T_N$.

We have calculated the dynamic correlation function for the staggered magnetization (a non-conserved order parameter) extracting the characteristic frequency and the associated dynamical index Z_N . We find, to $O(\epsilon)$, $Z_N = 2 - \epsilon/2$ in agreement with the RNG calculation of Halperin, Hohenberg, and Siggia.³ In three dimensions